Miniature pig model of human adolescent brain white matter development

Meghann C. Ryan[a], **Paul Sherman**[b], **Laura M. Rowland**[a], **S. Andrea Wijtenburg**[a], **Ashley Acheson**[c], **Els Fieremans**[d], **Jelle Veraart**[d], **Dmitry S. Novikov**[d], **L. Elliot Hong**[a], **John Sladky**[b,e], **P. Dana Peralta**[e], **Peter Kochunov**[a,*], and **Stephen A. McGuire**[b,e]

[a]Maryland Psychiatric Research Center, Department of Psychiatry, University of Maryland School of Medicine, 55 Wade Avenue, Catonsville, MD 21228, United States

[b]U.S. Air Force School of Aerospace Medicine, Aeromedical Research Department, 2510 5th Street, Building 840, Wright-Patterson AFB, OH 45433-7913, United States

[c]Department of Psychiatry, University of Arkansas for Medical Sciences, 4301 W Markham St, Little Rock, AR 72205, United States

[d]Center for Biomedical Imaging, Department of Radiology, New York University School of Medicine, 660 1st Avenue, New York, NY 10016, United States

[e]Department of Neurology, 59th Medical Wing, 2200 Bergquist Drive, Suite 1, Joint Base San Antonio-Lackland AFB, TX 78236, United States

Abstract

Background—Neuroscience research in brain development and disorders can benefit from an *in vivo* animal model that portrays normal white matter (WM) development trajectories and has a sufficiently large cerebrum for imaging with human MRI scanners and protocols.

New method—Twelve three-month-old Sinclair™ miniature pigs (*Sus scrofa domestica*) were longitudinally evaluated during adolescent development using advanced diffusion weighted imaging (DWI) focused on cerebral WM. Animals had three MRI scans every 23.95 ± 3.73 days using a 3-T scanner. The DWI imaging protocol closely modeled advanced human structural protocols and consisted of fifteen b-shells (b = 0–3500 s/mm^2) with 32-directions/shell. DWI data were analyzed using diffusion kurtosis and bi-exponential modeling that provided measurements that included fractional anisotropy (FA), radial kurtosis, kurtosis anisotropy (KA), axial kurtosis, tortuosity, and permeability-diffusivity index (PDI).

Results—Significant longitudinal effects of brain development were observed for whole-brain average FA, KA, and PDI (all p < 0.001). There were expected regional differences in trends, with corpus callosum fibers showing the highest rate of change.

---

*Corresponding author: pkochunov@mprc.umaryland.edu (P. Kochunov).

Comparison with existing method(s)—Pigs have a large, gyrencephalic brain that can be studied using clinical MRI scanners/protocols. Pigs are less complex than non-human primates thus satisfying the "replacement" principle of animal research.

Conclusions—Longitudinal effects were observed for whole-brain and regional diffusion measurements. The changes in diffusion measurements were interepreted as evidence for ongoing myelination and maturation of cerebral WM. Corpus callosum and superficial cortical WM showed the expected higher rates of change, mirroring results in humans.

Keywords

Diffusion weighted imaging; White matter; Miniature swine; Adolescent brain development

1. Introduction

Adolescence to early adulthood is a crucial period for human brain development that is associated with acquisition of higher cognitive functions and emergence of neuropsychiatric illnesses (Rapoport et al., 2005a; Casey et al., 2007; Kalia, 2008). Magnetic resonance imaging (MRI) based brain assessments have become the primary approach for studying human brain development, and there is a need for an animal model that allows equivalent neuroimaging to be complemented with invasive neuroscience techniques. However, the established animal models for brain development, including laboratory rodents and ferrets (Jacob, 1999; Bryda, 2013; Rosenthal and Brown, 2007; Hardouin and Nagy, 2000; Armstrong et al., 1991; Welker, 1990) and non-human primates (Goodman and Check, 2002; Bontrop, 2001; Torres et al., 2010; Patterson and Carrion, 2005; VandeBerg and Williams-Blangero, 1997), have significant limitations or challenges. Rats and mice have a lissencephalic cortex and their brains are different from human in both appearance and structural proportionality. Ferrets do have a gyrencephalic cortex, but their cerebral gyrification process differs from humans and occurs after birth (Smart and McSherry, 1986; Kochunov et al., 2010b). Further, the small brain volume of both rodents and ferrets necessitates the use of dedicated high-field, small-bore animal MRI scanners and special imaging protocols, which substantially reduces the potential for translational research. Non-human primates have a cerebral development pattern comparable to humans and can be studied using a human MRI scanner (Armstrong et al., 1991; Kochunov et al., 2010b; Armstrong et al., 1995; Pillay and Manger, 2007; Kochunov et al., 2011a); however, non-human primates are expensive and have ethical constraints that limit their availability for basic neuroscience research. Here, we tested the miniature pig (*Sus scrofa domestica*), as an animal model for translational neuroimaging studies of adolescent brain development that overcomes most of the above limitations.

Human brain development includes two critical periods separated in time: primary gyrification and primary myelination (Kochunov et al., 2010, 2009a). The primary gyrification starts during the third trimester and is completed by birth. During this period, the cortical folding coupled with cortical surface area expansion and the differentiation/ branching of axons and dendrites, leads to the creation of a gyrencephalic cortex (Xu et al., 2010; Bayly et al., 2014). Abnormalities in cortical folding are generally caused by genetic disorders and result in reduced cognitive ability (Bayly et al., 2014; Pang et al., 2008;

Nordahl et al., 2007; Hardan et al., 2004). Primary cerebral myelination begins soon after birth and continues until early adulthood (Flechsig, 1901a). It is a highly heterochronic process (Dubois et al., 2012; Kulikova et al., 2015; Dean et al., 2016, 2015, 2017; Lebel and Beaulieu, 2011; Lebel et al., 2012; Kinney et al., 1988; Barkovich et al., 1988) with motor and sensory WM bundles become fully myelinated during childhood (Lebel et al., 2008; Eluvathingal et al., 2007; Bonekamp et al., 2007; Ashtari et al., 2007; Barnea-Goraly et al., 2005; Schmithorst et al., 2002; Mukherjee et al., 2001). Myelinated axons in the brain's WM support its functionality by propagating electric signal transmissions through saltatory conductance (Hildebrand et al., 1993; Susuki, 2013; Miller et al., 2013). Thus, the myelination level impacts the propagation speed of the action potential (Lutz et al., 2005; Ashe and Georgopoulos, 1994; Bartzokis et al., 2010). In adolescence, changes in the fronto-cortical and fronto-striatal circuits lead to the development of higher cognitive skills (Bartzokis et al., 2010; Bartzokis, 2004; Bartzokis et al., 1999; Bastos Leite et al., 2004; Kochunov et al., 2010a; Kochunov et al., 2009b; Prins et al., 2004; Schiavone et al., 2009). Adolescence is also a peak period for the development of neuropsychiatric disorders, such as schizophrenia, and when reduced inhibition and excessive reward seeking and risky behaviors may lead to life-long substance use disorders (Weinberger and Lipska, 1995; Lewis and Levitt, 2002; Rapoport et al., 2012, 2005b; Murray et al., 1992; McGorry et al., 2011). Myelination of associative WM tracts improves connectivity of the intra-cortical connectivity networks and maximizes information processing speed and energy efficiency (Hildebrand et al., 1993; Harris and Attwell, 2012; Vaishnavi et al., 2010; Lee et al., 2012; Wen and Chklovskii, 2005; Laughlin and Sejnowski, 2003).

The miniature pig is commonly utilized in translational research pertaining to the cardiovascular, digestive, and integumentary systems (Stricker-Krongrad et al., 2016; Swindle et al., 2012; Schomberg et al., 2016) due to anatomical, physiological, and genetic similarities to humans (Swindle et al., 2012; Schomberg et al., 2016; Wernersson et al., 2005). The intermediate size of miniature pigs allows for easier housing (Stricker-Krongrad et al., 2016), and they are significantly less expensive than non-human primates (Schomberg et al., 2016; Coors et al., 2010). Miniature pigs are intelligent, have a mild temperament, and are amendable for training and cognitive research (Stricker-Krongrad et al., 2016; Schomberg et al., 2016). Miniature pigs have a fully gyrencephalic brain, undergo primary gyrification in-utero and as adults have an equal ratio of cerebral white and gray matter (Fig. 1), comparable to that in humans (Swindle et al., 2012; Schomberg et al., 2016; Conrad et al., 2012; Ostergaard et al., 1998). Further, miniature pigs and humans have analogous brain development, including similar myelination and brain white matter growth patterns (Sauleau et al., 2009).

We used quantitative diffusion weighted imaging (DWI) for longitudinal assessment of changes in cerebral WM in the adolescent-age miniature pigs. Diffusion tensor imaging (DTI) is the most commonly used DWI approach that describes the Gaussian properties of the diffusion displacement distribution of water in the brain by fitting a mono-exponential function to the weighted diffusion signal decay at a low "diffusion weighting" (b-value 1000 s/mm^2). The choice of a lower b-value range makes DTI sensitive to water molecules with high diffusivities. Neuroimaging studies in humans have mapped the normal developmental trajectory of cerebral WM using DTI's fractional anisotropy (FA) of water

diffusion (Kochunov et al., 2012; Flechsig, 1901b; Yakovlev and Lecours, 1967; Kochunov et al., 2011b; Gao et al., 2009; Ben Bashat et al., 2005). FA is also a valuable phenotype in neuropsychiatric disorders. Reduced FA has been found in adolescents with high clinical risk for development of psychosis (Karlsgodt et al., 2009, 2012, 2015), schizophrenia (Wright et al., 2015; Nazeri et al., 2013; Perez-Iglesias et al., 2010; Friedman et al., 2008; Alba-Ferrara and de Erausquin, 2013; Phillips et al., 2012; Kubicki et al., 2007; Glahn et al., 2013; Ellison-Wright and Bullmore, 2009), and substance use disorders (Acheson et al., 2015, 2014a,b). FA is a simple and empirical parameter but it lacks biological specificity and that makes interpretation of FA findings difficult (Alba-Ferrara and de Erausquin, 2013; Pierpaoli and Basser, 1996). Moreover, the water diffusion signal is non-Gaussian, and at higher b-values, DTI fails to approximate the non-mono-exponential decay of diffusion signal that is caused by the restriction of diffusion by cellular membranes (Jensen and Helpern, 2010; Sukstanskii et al., 2003, 2004). We supplemented DTI metrics with two DWI analysis methods: diffusion kurtosis imaging (DKI) (Jensen et al., 2005a) and permeability-diffusivity (PD) (Kochunov et al., 2013). DKI and PD models overcome the limitations of DTI and characterize the sources of the non-Gaussian distribution of diffusion signals.

In the present study, we hypothesized that the diffusion signal from white matter (WM) in the miniature pigs can serve as a good animal model for adolescent to young adult brain development in humans. Specifically, we used adolescent aged miniature pigs to (1) study the sensitivity of the different DWI measurements to adolescent development in whole-brain WM and (2) explore the WM regional heterochronicity to assess the different developmental trajectories in various brain regions.

2. Methods

2.1. Animal subjects

Twelve female Sinclair™ miniature swine underwent three MRI scans every 23.95 ± 3.73 days. Female swine were chosen to facilitate bladder catherization for the prolonged duration MRI. All remained free of disease throughout the duration of the study. The average ages for MRI #1, #2, and #3 were 102.58 ± 16.91 days, 123.58 ± 17.10 days, and 149.5 ± 15.96 days, respectively. The sample was age-selected to correspond with human adolescence/early adulthood (age 10–19 years). The pigs are considered late pre-pubescent for MRI #1 and sexually mature by MRI #3. Four of the twelve animals were transferred into another study prior to MRI #3 and one was missing DKI data on MRI #3. The local Institutional Animal Care and Use Committee reviewed and approved all animal protocols. All animals were housed in the 59th Clinical Research Division vivarium of Joint Base San Antonio Lackland Air Force Base (AFB), TX.

2.2. Imaging protocol

All imaging was performed using a Siemens 3-T Verio scanner with a multi-channel knee coil at the Wilford Hall Ambulatory Surgical Center, 59th Medical Wing, Joint Base San Antonio-Lackland AFB, TX. A human knee coil (inner diameter ~ 180 mm) provided an excellent coverage (field of view ~200 mm) for the brain and a comfortable fit for the animals placed in prone position. It provided a better signal-to-noise ratio (SNR) than

volumetric coils for human brain imaging, however, SNR may likely be improved by the use of custom RF coils optimized for miniature pig anatomy. General anesthesia in the form of isoflurane was administered with an MRI-compatible machine for the 3-h scan duration. Metabolic and fluid status was continuously monitored and no subjects displayed signs of distress. Pigs were imaged in the prone position.

2.3. Diffusion weighted imaging and data processing

The DWI protocol was developed based on q-space protocols for *in vivo* mapping of water diffusion in the brain (Wu et al., 2011; Clark et al., 2002). This protocol consisted of 15 shells of b-values (b = 0, 250, 500, 600, 700, 800, 900, 1000, 1250, 1500, 1750, 2000, 2500, 3000, 3500 s/mm^2; diffusion gradient duration = 47 ms, diffusion gradient separation = 54 ms). Thirty-two isotropically distributed diffusion weighted directions were collected per shell, including sixteen b = 0 images. Three dummy scans preceded the data collection to establish the steady state. The highest b-value (b = 3500 s/mm^2) was chosen because the signal-to-noise ratio (SNR) for the corpus callosum in the diffusion weighted image (SNR = 6.9 ± 0.7) measured during protocol development approached the empirically selected lower limit of SNR = 5.0. The b-values and the number of directions per shell were chosen for improved fit of the bi-exponential model and SNR (Jones et al., 1999). The imaging data were collected using a single-shot, echo-planar, single refocusing spin-echo, T2-weighted sequence with a spatial resolution of $1.72 \times 1.72 \times 1.70$ mm and 40 slices prescribed in axial orientation for complete brain coverage. The sequence was repeated with the reversal of the phase encoding gradients for correction of spatial distortions and improvement in SNR (Fig. 2). In addition to DWI, high-resolution (0.5-mm isotropic) T1-weighted structural data were collected.

Thermal noise in the data was reduced by applying the Marchenko Pastour Principle Component Analysis (MPPCA) denoising technique that exploits the inherent redundancy in diffusion MRI data (Veraart et al., 2016a,c,b). Thereafter, the data was corrected for Gibbs ringing (Kellner et al., 2016), Rician bias (Gudbjartsson and Patz, 1995), geometric eddy current and EPI distortions, and subject motion (Andersson and Sotiropoulos, 2016, 2015; Andersson et al., 2003; Smith et al., 2004).

2.3.1. DKI model calculations—DKI is a model-independent diffusion signal representation that extends conventional DTI by the addition of the kurtosis term to account for non-Gaussian behavior of the diffusion signal (Eq. (1), Fig. S1, see supplement) (Jensen and Helpern, 2010; Jensen et al., 2005b; Lu et al., 2006). Both the diffusion and kurtosis tensors can be derived from the second-order expansion of the multi **b**-shell diffusion-weighted signal decay as function of the **b**-value:

$$\ln S(b, \boldsymbol{g}) = \ln S(0) - b \sum_{i,j=1}^{3} g_i g_j D_{ij} + \frac{b^2}{6} \left(\sum_{i=1}^{3} \frac{D_{ii}}{3} \right)^2 \sum_{i,j,k,l=1}^{3} g_i g_j g_k g_l W_{ijkl} + O\left(b^3\right) \tag{1}$$

with g_i the ith component of gradient direction $\boldsymbol{g}$ and $S(0)$ the nondiffusion-weighted signal intensity. $\boldsymbol{D}_{ij}$ is the ijth element of the fully symmetric diffusion tensor $\boldsymbol{D}$, characterized by

six independent elements and W_{ijkl} denotes an element of the diffusion kurtosis tensor **W**, which is fully parameterized by 15 independent elements. The DKI model was fit based on the reduced set of diffusion values (b up to 2500s/mm2) to minimize approximation errors $O(b^3)$, yet to capture the non-Gaussian diffusion effect that become apparent at intermediate *b*-values.

During the model fit, multivariate regression was used to estimate the eigenvalues for the diffusion ($L_{1,2,3}$) and kurtosis ($K_{1,2,3}$) tensors. The three eigenvalues for diffusion tensor were converted to axial ($L_|$), radial, ($L_\perp$), and FA. Similarly, the three eigenvalues of the kurtosis tensor were converted to axial ($K_|$), radial, ($K_\perp$), and kurtosis anisotropy (KA) values (Poot et al., 2010)

2.3.2. Permeability-diffusivity model calculations—The PD model is based on the bi-exponential fit of diffusion decay (Eqs. (2) and (3)) (Kochunov et al., 2013):

$$\frac{S(b)}{S_0} + M_u \cdot e^{-b \cdot D_u} + (1 - M_u) \cdot e^{-b \cdot D_r} \frac{S(b)}{S_0} = M_u \cdot e^{-b \cdot D_u} + (1 - M_u) \cdot e^{-b \cdot D_r} \tag{2}$$

$$PDI = D_r \Big/ D_u \tag{3}$$

Here S(b) is a diffusion weighted signal for a given b value, averaged across all directions. M_u is the compartmental fraction of the signal that comes from unrestricted diffusion, and $(1–M_u)$ is the signal from the restricted diffusing compartment. D_u and D_r are the diffusivity of the unrestricted and restricted compartments, respectively. The expansion was fit based on the full set of diffusion values (0–3500 s/mm^2); using the following initial fit values: M_u = 0.5,. D_u = 0.1 and D_r = 0.01 mm2/s.

2.3.3. Global and regional diffusion measurements—All diffusion measurements were extracted using tract-based spatial statistics protocol by combining ENIGMA-DTI protocol (Jahanshad et al., 2013) with the piglet MRI brain atlas (Conrad et al., 2014). Briefly, T1-brain images were registered to the pig brain atlas using a 12-parameter transformation and the transformation was used to reslice FA images for individual brains. Next, a "minimal deformation target" was created based on FA images from the participating animals as previously described (Jahanshad et al., 2013). The data were then processed using FSL's tract-based spatial statistics (*TBSS*; http://fsl.fmrib.ox.ac.uk/fsl/fslwiki/TBSS) analytic method (Smith et al., 2006) modified to project individual FA values on the hand-segmented pig skeleton mask. After extracting the skeletonized WM, FA values corresponding to the middle of major WM tracts, based on the local maximum in the direction normal to the skeleton, were projected onto the WM skeleton. This analysis was repeated for images of the DKI and PD index (PDI) parameters using the non-FA option of the pipeline. This option produced skeletonized WM images of corresponding non-FA values. Following projection, regions of interest, derived from the pig brain atlas, were transferred to extract the mean values for the full skeleton and average values for major brain

areas, including the corpus callosum (CC) and superficial WM. Whole-brain averaged diffusion parameters were obtained by averaging the entire skeleton. Overall, the entire DWI imaging and DKI/PDI modeling approaches essentially remained the same as human DWI protocols (Kochunov et al., 2016a) to maximize the translational potential of the miniature pig model.

2.4. Statistical analyses

2.4.1. Regression analysis—To assess longitudinal trends in the diffusion measurements, we used a generalized linear mixed effects (GLME) model. The GLME model partitions the variance in the measurements from each subject into the fixed (predictor) effects that are observed on the group level and a random set of latent, non-independent effects that are individual to each subject. The normality of the distribution of the diffusion parameters were verified using Kolmogorov-Smirnov and Shapiro-Wilk statistics (all p > 0.2) Modeling longitudinal measurements using GLME models allows the results of the study to be more representative by accounting for non-independent individual variance. The GLME model is more flexible than repeated ANOVA analyses because it does not require the same number of measurements for each subject. The GLME modeling used age as the fixed predictor for the diffusion measurements and a random effect variable (ε) to account for individualized variance for each animal. This model is shown in Eq. (4):

$$\boldsymbol{P_{i,j}} = A + \beta_{Age} \cdot Age_{i,j} + \alpha_{i,j} \quad (4)$$

where $P_{i,j}$ is the diffusion parameter (FA, KA, AK, AD, RD, or PDI) for the "jth" pig at the age ($Age_{i,j}$) in days since birth of the "ith" imaging session, A is a constant, β is the regression coefficient, and $\alpha_{i,j}$ is a mixed effect coefficient.

GLME modeling was performed in R (R-Development-Core-Team., 2009) using the nonlinear mixed effect model library (nlme) (Pinheiro et al., 2012). The model accounts for variance between subjects by determining both the fixed and random effects. Linearity between the diffusion measurements and age is established before outputting the standardized regression coefficients (β) and standard errors.

For the regional measurements, Bonferroni correction set statistical significance at p 0.007 to reduce type 1 errors associated with multiple (N = 7 brain regions) comparisons; p-values between 0.008 and 0.05 were deemed suggestively significant and were also discussed.

3. Results

3.1. Whole-brain longitudinal trends

Significant longitudinal effects of age were observed for FA, KA and PDI (all p < 0.001) (Table 1, Fig. 3). All three diffusion measurements showed consistent longitudinal rise with age, except for one animal (Fig. 3). Significant decreases with age were observed for axial kurtosis (AK) and radial kurtosis (RK) (p = 0.027 and 0.025, respectively) (Fig. 4)**.** The radial diffusivity showed a negative trend but it was not significant (Fig. S2). The average

FA was significantly and positively correlated with both KA and PDI (r = 0.59 and 0.40, p < 0.001). KA and PDI were also significantly correlated (r = 0.81, p < 10^{-8}).

3.2. Regional longitudinal trends

Regional effects of aging were assessed using diffusion metrics obtained for six brain areas from the piglet brain atlas (Conrad et al., 2014): CC, superficial WM, parahippocampal WM, midbrain, thalamic radiation (TR), and internal/external capsule (I/EC) (Table 2). Measures from the left and right hemispheres of the same structure were averaged, as there was no evidence of significant lateralization.

Significant longitudinal changes in DWI parameters were observed for all brain regions except for the parahippocampal WM which showed no age effects on any of the diffusion measurements. FA and KA increased in all regions except for the parahippocampal WM, and PDI significantly increased in the CC, superficial WM, midbrain, and TR. RK significantly decreased in the midbrain and TR. The PDI increase in the corpus callosum was the most robust effect observed (p = 6.7 10^{-7}), followed by the rise in KA in the TR (p = 1.4 10^{-6}) and the rise in FA in the I/EC (p = 5.6 10^{-6}). Except for AK and RK, the diffusion metrics increased with age.

4. Discussion

A longitudinal imaging protocol was used to assess changes in WM integrity during normal adolescent maturation in miniature pigs. The trends of WM DWI measurements were similar to these observed during the period of adolescence and young adulthood in humans (Kochunov et al., 2012; Grinberg et al., 2017; Howroyd et al., 2016; Peter et al., 2016). In addition to the rise in DTI-FA values, we observed significant changes in two DWI parameters that describe the non-Gaussian diffusion properties KA and PDI. We interpreted these changes based on findings in humans as evidence for ongoing structural maturation of cerebral WM. Also, analogous to humans, the highest rates of change were observed in the CC and superficial WM, suggesting heterochronicity of WM development in pigs (Kochunov et al., 2012, 2011b).

We are developing the miniature pig adolescent WM development model to complement existing small animal laboratory models including rats (Crum et al., 2017; Hansen et al., 2017; Lentz et al., 2014; Petrenko et al., 2017) and ferrets (Das and Takahashi, 2017; Hutchinson et al., 2016; Knutsen et al., 2010; Schwerin et al., 2017). Large, gyrencephalic brains of miniature pigs can be studied using a human MRI scanner and imaging protocols developed for human subjects (Kochunov et al., 2013, 2014). The lower costs and shorter development span for the miniature pig model compares favorably with the non-human primate research models of brain development (Kochunov et al., 2010b, 2011a; Kohama et al., 2012; Li et al., 2017; Sakai et al., 2017a,b). Miniature pigs are sexually mature by six months of age, while it may take 4–5 years for non-human primates to reach that developmental landmark (Onyango et al., 2013; Abee, 2017). The gestational period for miniature pigs is likewise shorter, lasting only 16 weeks (McAnulty et al., 2017) compared to 38 weeks for non-human primates (Onyango et al., 2013; Abee, 2017). Mice have a shorter (three week) gestational period and are sexually mature between 5 and 8 weeks of

age (Lambert, 2007). However, weaning of mice at 3 weeks of age shortens the opportunity for pre-/adolescent development research to 2–5 weeks. Miniature pigs are weaned at 6–8 weeks of age and therefore, longer, but still compressed, development period posits a miniature pig as a valuable research model for adolescent development.

We observed significant increases in FA in pigs, similar to these reported during adolescent development in humans. FA is a non-specific index that reflects the anisotropy of the Gaussian diffusivity of the fast diffusing water pool (Kochunov et al., 2013). The non-specific nature of this index renders interpretation of changes in FA speculative. For example, increases in FA values may be due to increased myelination of WM microstructures and can be considered an indirect measurement of myelin level (Budde et al., 2007; Madler et al., 2008; Song et al., 2003, 2005). A decrease in RD, a parameter that reflects water movement perpendicular to the fiber axis, reinforces this interpretation. In pigs, RD showed a decreasing trend with age, but was not statistically significant due to higher variance in this measurement. However, FA is also sensitive to reorganization of white matter fibers including changes in axon diameter, axonal density, and/or membrane permeability (Beaulieu, 2002; Jones and Cercignani, 2010; Jones et al., 2013; Takahashi et al., 2002).

Advancements in DWI technology provide for a noninvasive, quantitative analysis of non-Gaussian diffusion indexes to portray developmental trajectories that correspond to changes in the slow diffusing pool of water that are sensitive to membrane permeability, axonal growth, and maturation (Lebel et al., 2008; Barnea-Goraly et al., 2005; Kochunov et al., 2013). Overall, our findings are suggestive of cerebral WM maturation and are consistent with the study performed by Grinberg and colleagues, who showed significant changes in Gaussian and non-Gaussian DWI parameters with age in adolescent humans (Grinberg et al., 2017). The DTI-FA, DKI-KA and PDI rose significantly with age in pigs, similar to the trends observed in humans (Grinberg et al., 2017). The DTI, DKI and PD techniques provide convenient mathematical representation of the signal but make no specific assumptions regarding the underlying biophysical phenomena. The derived diffusion metrics should primarily be discussed in a phenomenological way, without necessarily referring to specific biological postulations of the model features, but taking advantage of the measurements in the extended range of b-values and bi-exponential fits (Grinberg et al., 2011). The robust and significant changes in the FA, KA and PDI during maturation encourage basic neuroscience and biophysics efforts to identify the water diffusion mechanisms governing these DWI signal.

Analysis of regional diffusion trends suggested that pigs may have a heterochronic WM development pattern. In humans, WM development is highly heterochronic (Dubois et al., 2012; Kulikova et al., 2015; Dean et al., 2016, 2015, 2017; Lebel and Beaulieu, 2011; Lebel et al., 2012; Kinney et al., 1988; Barkovich et al., 1988). The motor and sensory WM bundles in humans become fully myelinated during childhood (Lebel et al., 2008; Eluvathingal et al., 2007; Bonekamp et al., 2007; Ashtari et al., 2007; Barnea-Goraly et al., 2005; Schmithorst et al., 2002; Mukherjee et al., 2001). In contrast, the associative WM tracts develop into the third and fourth decades of life (Barkovich et al., 1988; Lebel et al., 2008; Eluvathingal et al., 2007; Bonekamp et al., 2007; Ashtari et al., 2007; Barnea-Goraly

et al., 2005; Schmithorst et al., 2002; Mukherjee et al., 2001), well past the average age of onset for schizophrenia and other neuropsychiatric disorders (Flechsig, 1901a; Yakovlev and Lecours, 1967; Kochunov and Hong, 2014; Kochunov et al., 2016b).

There are few DTI studies on normal longitudinal white matter development in mice (Zhang et al., 2006; Larvaron et al., 2007). Small brain size and limited spatial resolution prevents visualization of WM tracts and DTI imaging in mice is susceptible to partial volume effects of GM/WM tissue and cerebral spinal fluid (Larvaron et al., 2007; Wu et al., 2013). Only limited DTI research was conducted in ferrets due to similar limitations (Hutchinson et al., 2016; Kroenke et al., 2009; Bock et al., 2010; Tao et al., 2012; Olavarria et al., 2012; Hutchinson et al., 2017).

There are several limitations in this pilot study. First, an all-female pig population was used due to ease of bladder catherization. Prior studies have established significant brain maturation differences between the sexes, including development rates and brain-volume differences (Eluvathingal et al., 2007; Luders et al., 2005; Allen et al., 2003; Durston et al., 2001). This study is also limited by a small number of animals and the use of a coarse, piglet brain atlas. Investigations with a larger sample size would allow for timing comparisons amongst the regional trajectory rates. Future development should also include a detailed atlas of cerebral WM tracts in pigs that is validated with histological measurements to map the brain development trends from birth to maturity.

5. Conclusion

We demonstrated the applicability of an advanced DWI protocol in pigs and showed agreement in trends and heterochronicity between adolescent development in pigs and humans. The fully gyrencephalic brain and prolonged WM maturation make the miniature pig a more accurate model of human development than small laboratory animals, and low costs and a shorter period of cerebral development make it a good alternative to non-human primate. A limitation of all animal models is the ability to translate research findings to the humans and the use of animal-specific MRI scanners and sequences may delay translation. The benefit of a miniature pig model is that human scanners/protocols can be used for collecting neuroimaging indices in an animal model that permits basic neuroscience research. We demonstrated the potential use of miniature pigs as an animal model for neuroimaging studies of brain development. Additional applications of this model may include traumatic brain/diffuse axonal injury, neuroinflammation and other neuroimaging translational research studies that require large gyrencephalic animal models.

Supplementary Material

Refer to Web version on PubMed Central for supplementary material.

Acknowledgments

References

Abee, CR. Nonhuman Primates in Biomedical Research: Biology and Management. Elsevier; 2017. 2012

Acheson A, et al. Combining diffusion tensor imaging and magnetic resonance spectroscopy to study reduced frontal white matter integrity in youths with family histories of substance use disorders. Hum Brain Mapp. 2014a; 35(12):5877–5887. [PubMed: 25044331]

Acheson A, et al. Assessment of whole brain white matter integrity in youths and young adults with a family history of substance-use disorders. Hum Brain Mapp. 2014b; 35(11):5401–5413. [PubMed: 24867528]

Acheson A, et al. Striatal activity and reduced white matter increase frontal activity in youths with family histories of alcohol and other substance-use disorders performing a go/no-go task. Brain Behav. 2015; 5(7):e00352. [PubMed: 26221573]

Alba-Ferrara LM, de Erausquin GA. What does anisotropy measure? Insights from increased and decreased anisotropy in selective fiber tracts in schizophrenia. Front Integr Neurosci. 2013; 7:9. [PubMed: 23483798]

Allen JS, et al. Sexual dimorphism and asymmetries in the gray-white composition of the human cerebrum. Neuroimage. 2003; 18(4):880–894. [PubMed: 12725764]

Andersson JL, Sotiropoulos SN. Non-parametric representation and prediction of single- and multi-shell diffusion-weighted MRI data using Gaussian processes. Neuroimage. 2015; 122:166–176. [PubMed: 26236030]

Andersson JLR, Sotiropoulos SN. An integrated approach to correction for off-resonance effects and subject movement in diffusion MR imaging. Neuroimage. 2016; 125:1063–1078. [PubMed: 26481672]

Andersson JL, Skare S, Ashburner J. How to correct susceptibility distortions in spin-echo-planar images: application to diffusion tensor imaging. Neuroimage. 2003; 20(2):870–888. [PubMed: 14568458]

Armstrong E, et al. Cortical gyrification in the rhesus monkey: a test of the mechanical folding hypothesis. Cereb Cortex. 1991; 1(5):426–432. [PubMed: 1822750]

Armstrong E, et al. The ontogeny of human gyrification. Cereb Cortex. 1995; 5(1):56–63. [PubMed: 7719130]

Ashe J, Georgopoulos AP. Movement parameters and neural activity in motor cortex and area 5. Cereb Cortex. 1994; 4(6):590–600. [PubMed: 7703686]

Ashtari M, et al. White matter development during late adolescence in healthy males: a cross-sectional diffusion tensor imaging study. Neuroimage. 2007; 35(2):501–510. [PubMed: 17258911]

Barkovich AJ, et al. Normal maturation of the neonatal and infant brain: MR imaging at 1.5 T. Radiology. 1988; 166(1 Pt 1):173–180. [PubMed: 3336675]

Barnea-Goraly N, et al. White matter development during childhood and adolescence: a cross-sectional diffusion tensor imaging study. Cereb Cortex. 2005; 15(12):1848–1854. [PubMed: 15758200]

Bartzokis G, et al. MRI evaluation of brain iron in earlier- and later-onset Parkinson's disease and normal subjects. Magn Reson Imaging. 1999; 17(2):213–222. [PubMed: 10215476]

Bartzokis G, Lu PH, Tingus K, Mendez MF, Richard A, Peters DG, Oluwadara B, Barrall KA, Finn JP, Villablanca P, Thompson PM, Mintz J. Lifespan trajectory of myelin integrity and maximum

motor speed. Neurobiol Aging. 2010 Sep; 31(9):1554–1562. http://dx.doi.org/10.1016/j.neurobiolaging.2008.08.015, Epub 2008 Oct 15. [PubMed: 18926601]

Bartzokis G. Age-related myelin breakdown: a developmental model of cognitive decline and Alzheimer's disease. Neurobiol Aging. 2004; 25(1):5–18. [PubMed: 14675724]

Bastos Leite AJ, Scheltens P, Barkhof F. Pathological aging of the brain: an overview. Top Magn Reson Imaging. 2004; 15(6):369–389. [PubMed: 16041289]

Bayly PV, Taber LA, Kroenke CD. Mechanical forces in cerebral cortical folding: a review of measurements and models. J Mech Behav Biomed Mater. 2014; 29:568–581. [PubMed: 23566768]

Beaulieu C. The basis of anisotropic water diffusion in the nervous system –a technical review. NMR Biomed. 2002; 15(7–8):435–455. [PubMed: 12489094]

Ben Bashat D, et al. Normal white matter development from infancy to adulthood: comparing diffusion tensor and high b value diffusion weighted MR images. J Magn Reson Imaging. 2005; 21(5):503–511. [PubMed: 15834918]

Bock AS, et al. Diffusion tensor imaging detects early cerebral cortex abnormalities in neuronal architecture induced by bilateral neonatal enucleation: an experimental model in the ferret. Front Syst Neurosci. 2010; 4:149. [PubMed: 21048904]

Bonekamp D, et al. Diffusion tensor imaging in children and adolescents: reproducibility, hemispheric, and age-related differences. Neuroimage. 2007; 34(2):733–742. [PubMed: 17092743]

Bontrop RE. Non-human primates: essential partners in biomedical research. Immunol Rev. 2001; 183:5–9. [PubMed: 11782243]

Bryda EC. The Mighty Mouse: the impact of rodents on advances in biomedical research. Mo Med. 2013; 110(3):207–211. [PubMed: 23829104]

Budde MD, et al. Toward accurate diagnosis of white matter pathology using diffusion tensor imaging. Magn Reson Med. 2007; 57(4):688–695. [PubMed: 17390365]

Casey BJ, Nigg JT, Durston S. New potential leads in the biology and treatment of attention deficit-hyperactivity disorder. Curr Opin Neurol. 2007; 20(2):119–124. [PubMed: 17351480]

Clark CA, Hedehus M, Moseley ME. In vivo mapping of the fast and slow diffusion tensors in human brain. Magn Reson Med. 2002; 47(4):623–628. [PubMed: 11948721]

Conrad MS, Dilger RN, Johnson RW. Brain growth of the domestic pig (Sus scrofa) from 2 to 24 weeks of age: a longitudinal MRI study. Dev Neurosci. 2012; 34(4):291–298. [PubMed: 22777003]

Conrad MS, et al. An in vivo three-dimensional magnetic resonance imaging-based averaged brain collection of the neonatal piglet (Sus scrofa). PLoS One. 2014; 9(9):e107650. [PubMed: 25254955]

Coors ME, et al. The ethics of using transgenic non-human primates to study what makes us human. Nat Rev Genet. 2010; 11(9):658–662. [PubMed: 20717156]

Crum WR, et al. Evolution of structural abnormalities in the rat brain following in utero exposure to maternal immune activation: a longitudinal in vivo MRI study. Brain Behav Immun. 2017; 63:50–59. [PubMed: 27940258]

Das A, Takahashi E. Characterization of white matter tracts by diffusion MR tractography in cat and ferret that have similar gyral patterns. Cereb Cortex. 2017:1–10.

Dean DC 3rd, et al. Characterizing longitudinal white matter development during early childhood. Brain Struct Funct. 2015; 220(4):1921–1933. [PubMed: 24710623]

Dean DC 3rd, et al. Mapping an index of the myelin g-ratio in infants using magnetic resonance imaging. Neuroimage. 2016; 132:225–237. [PubMed: 26908314]

Dean DC 3rd, et al. Mapping white matter microstructure in the one month human brain. Sci Rep. 2017:9759. [PubMed: 28852074]

Dubois J, et al. Brain development of infant and MRI by diffusion tensor imaging. Neurophysiol Clin. 2012; 42(1–2):1–9. [PubMed: 22200336]

Durston S, et al. Anatomical MRI of the developing human brain: what have we learned? J Am Acad Child Adolesc Psychiatry. 2001; 40(9):1012–1020. [PubMed: 11556624]

Ellison-Wright I, Bullmore E. Meta-analysis of diffusion tensor imaging studies in schizophrenia. Schizophr Res. 2009; 108(1–3):3–10. [PubMed: 19128945]

Eluvathingal TJ, et al. Quantitative diffusion tensor tractography of association and projection fibers in normally developing children and adolescents. Cereb Cortex. 2007; 17(12):2760–2768. [PubMed: 17307759]

Flechsig P. Developmental (myelogenetic) localisation of the cerebral cortex in the human. Lancet. 1901a; 158:1027–1030.

Flechsig P. Developmental (myelogenetic) localization of the cerebral cortex in the human subject. Lancet. 1901b; 158(4077):1027–1030.

Friedman JI, et al. Diffusion tensor imaging findings in first-episode and chronic schizophrenia patients. Am J Psychiatry. 2008; 165(8):1024–1032. [PubMed: 18558643]

Gao W, et al. Temporal and spatial development of axonal maturation and myelination of white matter in the developing brain. AJNR Am J Neuroradiol. 2009; 30(2):290–296. [PubMed: 19001533]

Glahn DC, et al. Genetic basis of neurocognitive decline and reduced white-matter integrity in normal human brain aging. Proc Natl Acad Sci U S A. 2013; 110(47):19006–19011. [PubMed: 24191011]

Goodman S, Check E. The great primate debate. Nature. 2002; 417(6890):684–687. [PubMed: 12066153]

Grinberg F, et al. Non-Gaussian diffusion in human brain tissue at high b-factors as examined by a combined diffusion kurtosis and biexponential diffusion tensor analysis. Neuroimage. 2011; 57(3): 1087–1102. [PubMed: 21596141]

Grinberg F, et al. Diffusion kurtosis metrics as biomarkers of microstructural development: a comparative study of a group of children and a group of adults. Neuroimage. 2017; 144(Pt A):12–22. [PubMed: 27639358]

Gudbjartsson H, Patz S. The Rician distribution of noisy MRI data. Magn Reson Med. 1995; 34(6): 910–914. [PubMed: 8598820]

Hansen B, et al. White matter biomarkers from fast protocols using axially symmetric diffusion kurtosis imaging. NMR Biomed. 2017; 30(9)

Hardan AY, et al. Increased frontal cortical folding in autism: a preliminary MRI study. Psychiatry Res. 2004; 131(3):263–268. [PubMed: 15465295]

Hardouin SN, Nagy A. Mouse models for human disease. Clin Genet. 2000; 57(4):237–244. [PubMed: 10845564]

Harris JJ, Attwell D. The energetics of CNS white matter. J Neurosci. 2012; 32(1):356–371. [PubMed: 22219296]

Hildebrand C, et al. Myelinated nerve fibres in the CNS. Prog Neurobiol. 1993; 40(3):319–384. [PubMed: 8441812]

Howroyd PC, Peter B, de Rijk E. Review of sexual maturity in the minipig. Toxicol Pathol. 2016; 44(4):607–611. [PubMed: 27102651]

Hutchinson EB, et al. Quantitative MRI and DTI abnormalities during the acute period following CCI in the ferret. Shock. 2016; 46(3 Suppl 1):167–176. [PubMed: 27294688]

Hutchinson EB, et al. Population based MRI and DTI templates of the adult ferret brain and tools for voxelwise analysis. Neuroimage. 2017; 152:575–589. [PubMed: 28315740]

Jacob HJ. Functional genomics and rat models. Genome Res. 1999; 9(11):1013–1016. [PubMed: 10568741]

Jahanshad N, et al. Multi-site genetic analysis of diffusion images and voxelwise heritability analysis: a pilot project of the ENIGMA-DTI working group. Neuroimage. 2013; 81:455–469. [PubMed: 23629049]

Jensen JH, Helpern JA. MRI quantification of non-Gaussian water diffusion by kurtosis analysis. NMR Biomed. 2010; 23(7):698–710. [PubMed: 20632416]

Jensen JH, et al. Diffusional kurtosis imaging: the quantification of non-gaussian water diffusion by means of magnetic resonance imaging. Magn Reson Med. 2005a; 53(6):1432–1440. [PubMed: 15906300]

Jensen JH, et al. Diffusional kurtosis imaging: the quantification of non-gaussian water diffusion by means of magnetic resonance imaging. Magn Reson Med. 2005b; 53(6):1432–1440. [PubMed: 15906300]

Jones DK, Cercignani M. Twenty-five pitfalls in the analysis of diffusion MRI data. NMR Biomed. 2010; 23(7):803–820. [PubMed: 20886566]

Jones DK, Horsfield MA, Simmons A. Optimal strategies for measuring diffusion in anisotropic systems by magnetic resonance imaging. Magn Reson Med. 1999; 42(3):515–525. [PubMed: 10467296]

Jones DK, Knosche TR, Turner R. White matter integrity, fiber count, and other fallacies: the do's and don'ts of diffusion MRI. Neuroimage. 2013; 73:239–254. [PubMed: 22846632]

Kalia M. Brain development: anatomy, connectivity, adaptive plasticity, and toxicity. Metabolism. 2008; 57(Suppl 2):S2–5. [PubMed: 18803960]

Karlsgodt KH, et al. White matter integrity and prediction of social and role functioning in subjects at ultra-high risk for psychosis. Biol Psychiatry. 2009; 66(6):562–569. [PubMed: 19423081]

Karlsgodt KH, et al. The relationship of developmental changes in white matter to the onset of psychosis. Curr Pharm Des. 2012; 18(4):422–433. [PubMed: 22239573]

Karlsgodt KH, et al. The accumbofrontal tract: diffusion tensor imaging characterization and developmental change from childhood to adulthood. Hum Brain Mapp. 2015; 36(12):4954–4963. [PubMed: 26366528]

Kellner E, et al. Gibbs-ringing artifact removal based on local subvoxel-shifts. Magn Reson Med. 2016; 76(5):1574–1581. [PubMed: 26745823]

Kinney HC, et al. Sequence of central nervous system myelination in human infancy: II. Patterns of myelination in autopsied infants. J Neuropathol Exp Neurol. 1988; 47(3):217–234. [PubMed: 3367155]

Knutsen AK, et al. A new method to measure cortical growth in the developing brain. J Biomech Eng. 2010; 132(10):101004. [PubMed: 20887014]

Kochunov P, Hong LE. Neurodevelopmental and neurodegenerative models of schizophrenia: white matter at the center stage. Schizophr Bull. 2014; 40(4):721–728. [PubMed: 24870447]

Kochunov P, et al. Genetics of primary cerebral gyrification: heritability of length, depth and area of primary sulci in an extended pedigree of Papio baboons. Neuroimage. 2009a; 15(53):1126–1132.

Kochunov P, et al. Can structural MRI cerebral health markers track cognitive trends in executive control function during normal maturation and adulthood? Hum Brain Mapp. 2009b; 30(8):2581–2594. [PubMed: 19067326]

Kochunov P, Coyle T, Lancaster J, Robin DA, Hardies J, Kochunov V, Bartzokis G, Stanley J, Royall D, Schlosser AE, Null M, Fox PT. Processing speed is correlated with cerebral health markers in the frontal lobes as quantified by neuroimaging. Neuroimage. 2010a January ;49(2):1190–1199. [PubMed: 19796691]

Kochunov P, et al. Mapping primary gyrogenesis during fetal development in primate brains: high-resolution in utero structural MRI of fetal brain development in pregnant baboons. Front Neurosci. 2010b; 4:20. [PubMed: 20631812]

Kochunov P, et al. Fetal brain during a binge drinking episode: a dynamic susceptibility contrast MRI fetal brain perfusion study. Neuroreport. 2011a; 21(10):716–721.

Kochunov P, et al. Fractional anisotropy of cerebral white matter and thickness of cortical gray matter across the lifespan. Neuroimage. 2011b; 58(1):41–49. [PubMed: 21640837]

Kochunov P, et al. Fractional anisotropy of water diffusion in cerebral white matter across the lifespan. Neurobiol Aging. 2012; 33(1):9–20. [PubMed: 20122755]

Kochunov P, Chiappelli J, Hong LE. Permeability-diffusivity modeling vs: fractional anisotropy on white matter integrity assessment and application in schizophrenia. Neuroimage Clin. 2013; 3:18–26. [PubMed: 24179845]

Kochunov P, et al. Multimodal white matter imaging to investigate reduced fractional anisotropy and its age-related decline in schizophrenia. Psychiatry Res. 2014; 223(2):148–156. [PubMed: 24909602]

Kochunov P, et al. Diffusion-weighted imaging uncovers likely sources of processing-speed deficits in schizophrenia. Proc Natl Acad Sci U S A. 2016a; 113(47):13504–13509. [PubMed: 27834215]

Kochunov P, Ganjgahi H, Winkler A, Kelly S, Shukla DK, Du X, Jahanshad N, Rowland L, Sampath H, Patel B, O'Donnell P, Xie Z, Paciga SA, Schubert CR, Chen J, Zhang G, Thompson PM, Nichols TE, Hong LE. Heterochronicity of white matter development and aging explains regional

patient control differences in schizophrenia. Hum Brain Mapp. 2016b December ;37(12):4673–4688. [PubMed: 27477775]

Kohama SG, Rosene DL, Sherman LS. Age-related changes in human and non-human primate white matter: from myelination disturbances to cognitive decline. Age (Dordr). 2012; 34(5):1093–1110. [PubMed: 22203458]

Kroenke CD, et al. Regional patterns of cerebral cortical differentiation determined by diffusion tensor MRI. Cereb Cortex. 2009; 19(12):2916–2929. [PubMed: 19363145]

Kubicki M, et al. A review of diffusion tensor imaging studies in schizophrenia. J Psychiatr Res. 2007; 41(1–2):15–30. [PubMed: 16023676]

Kulikova S, et al. Multi-parametric evaluation of the white matter maturation. Brain Struct Funct. 2015; 220(6):3657–3672. [PubMed: 25183543]

Lambert, R. Breeding Strategies for Maintaining Colonies of Laboratory Mice. The Jackson Laboratory; 2007.

Larvaron P, et al. In vivo analysis of the post-natal development of normal mouse brain by DTI. NMR Biomed. 2007; 20(4):413–421. [PubMed: 17120295]

Laughlin SB, Sejnowski TJ. Communication in neuronal networks. Science. 2003; 301(5641):1870–1874. [PubMed: 14512617]

Lebel C, Beaulieu C. Longitudinal development of human brain wiring continues from childhood into adulthood. J Neurosci. 2011; 31(30):10937–10947. [PubMed: 21795544]

Lebel C, et al. Microstructural maturation of the human brain from childhood to adulthood. Neuroimage. 2008; 40(3):1044–1055. [PubMed: 18295509]

Lebel C, et al. Diffusion tensor imaging of white matter tract evolution over the lifespan. Neuroimage. 2012; 60(1):340–352. [PubMed: 22178809]

Lee Y, et al. Oligodendroglia metabolically support axons and contribute to neurodegeneration. Nature. 2012; 487(7408):443–448. [PubMed: 22801498]

Lentz MR, et al. Diffusion tensor and volumetric magnetic resonance measures as biomarkers of brain damage in a small animal model of HIV. PLoS One. 2014; 9(8):e105752. [PubMed: 25144656]

Lewis DA, Levitt P. Schizophrenia as a disorder of neurodevelopment. Annu Rev Neurosci. 2002; 25:409–432. [PubMed: 12052915]

Li Q, et al. Chronic ketamine exposure causes white matter microstructural abnormalities in adolescent cynomolgus monkeys. Front Neurosci. 2017; 11:285. [PubMed: 28579941]

Lu H, et al. Three-dimensional characterization of non-gaussian water diffusion in humans using diffusion kurtosis imaging. NMR Biomed. 2006; 19(2):236–247. [PubMed: 16521095]

Luders E, et al. Mapping cortical gray matter in the young adult brain: effects of gender. Neuroimage. 2005; 26(2):493–501. [PubMed: 15907306]

Lutz K, et al. Asymmetry of cortical activation during maximum and convenient tapping speed. Neurosci Lett. 2005; 373(1):61–66. [PubMed: 15555778]

Madler B, et al. Is diffusion anisotropy an accurate monitor of myelination? Correlation of multicomponent T2 relaxation and diffusion tensor anisotropy in human brain. Magn Reson Imaging. 2008; 26(7):874–888. [PubMed: 18524521]

McAnulty, PA., et al. 2017 The Minipig in Biomedical Research. Taylor & Francis; 2011.

McGorry PD, et al. Age of onset and timing of treatment for mental and substance use disorders: implications for preventive intervention strategies and models of care. Curr Opin Psychiatry. 2011; 24(4):301–306. [PubMed: 21532481]

Miller DJ, et al. Prolonged myelination in human neocortical evolution. Proc Natl Acad Sci U S A. 2013; 109(41):16480–16485.

Mukherjee P, et al. Normal brain maturation during childhood: developmental trends characterized with diffusion-tensor MR imaging. Radiology. 2001; 221(2):349–358. [PubMed: 11687675]

Murray RM, et al. A neurodevelopmental approach to the classification of schizophrenia. Schizophr Bull. 1992; 18(2):319–332. [PubMed: 1377834]

Nazeri A, et al. Alterations of superficial white matter in schizophrenia and relationship to cognitive performance. Neuropsychopharmacology. 2013; 38(10):1954–1962. [PubMed: 23591167]

Nordahl CW, et al. Cortical folding abnormalities in autism revealed by surface-based morphometry. J Neurosci. 2007; 27(43):11725–11735. [PubMed: 17959814]

Olavarria JF, et al. Deafferentation-induced plasticity of visual callosal connections: predicting critical periods and analyzing cortical abnormalities using diffusion tensor imaging. Neural Plast. 2012; 2012:250196. [PubMed: 23213572]

Onyango PO, et al. Puberty and dispersal in a wild primate population. Horm Behav. 2013; 64(2):240–249. [PubMed: 23998668]

Ostergaard L, et al. Absolute cerebral blood flow and blood volume measured by magnetic resonance imaging bolus tracking: comparison with positron emission tomography values. J Cereb Blood Flow Metab. 1998; 18(4):425–432. [PubMed: 9538908]

Pang T, Atefy R, Sheen V. Malformations of cortical development. Neurologist. 2008; 14(3):181–191. [PubMed: 18469675]

Patterson JL, Carrion R Jr. Demand for nonhuman primate resources in the age of biodefense. ILAR J. 2005; 46(1):15–22. [PubMed: 15644560]

Perez-Iglesias R, et al. White matter integrity and cognitive impairment in first-episode psychosis. Am J Psychiatry. 2010; 167(4):451–458. [PubMed: 20160006]

Peter B, et al. Sexual maturation in the female gottingen minipig. Toxicol Pathol. 2016; 44(3):482–485. [PubMed: 26883154]

Petrenko V, et al. Multimodal MRI imaging of apoptosis-Triggered microstructural alterations in the postnatal cerebral cortex. Cereb Cortex. 2017:1–14.

Phillips KA, et al. Genetic contributions to the midsagittal area of the corpus callosum. Twin Res Hum Genet. 2012; 15(3):315–323. [PubMed: 22856367]

Pierpaoli C, Basser PJ. Toward a quantitative assessment of diffusion anisotropy. Magn Reson Med. 1996; 36(6):893–906. [PubMed: 8946355]

Pillay P, Manger PR. Order-specific quantitative patterns of cortical gyrification. Eur J Neurosci. 2007; 25(9):2705–2712. [PubMed: 17459107]

Pinheiro, J., et al. The Nlme Package: Linear and Nonlinear Mixed Effects Models, R Version 3. 2012.

Poot DH, et al. Optimal experimental design for diffusion kurtosis imaging. IEEE Trans Med Imaging. 2010; 29(3):819–829. [PubMed: 20199917]

Prins ND, et al. Cerebral white matter lesions and the risk of dementia. Arch Neurol. 2004; 61(10):1531–1534. [PubMed: 15477506]

R-Development-Core-Team. R: A Language and Environment for Statistical Computing. 2009. Available from: http://www.R-project.org

Rapoport JL, Addington A, Frangou S. The neurodevelopmental model of schizophrenia: what can very early onset cases tell us? Curr Psychiatry Rep. 2005a; 7(2):81–82. [PubMed: 15802082]

Rapoport JL, et al. The neurodevelopmental model of schizophrenia: update 2005. Mol Psychiatry. 2005b; 10(5):434–449. [PubMed: 15700048]

Rapoport JL, Giedd JN, Gogtay N. Neurodevelopmental model of schizophrenia: update 2012. Mol Psychiatry. 2012; 17(12):1228–1238. [PubMed: 22488257]

Rosenthal N, Brown S. The mouse ascending: perspectives for human-disease models. Nat Cell Biol. 2007; 9(9):993–999. [PubMed: 17762889]

Sakai T, Komaki Y, Hata J, Okahara J, Okahara N, Inoue T, Mikami A, Matsui M, Oishi K, Sasaki E, Okano H. Elucidation of developmental patterns of marmoset corpus callosum through a comparative MRI in marmosets, chimpanzees, and humans. Neurosci Res. 2017a; 122(September):25–34. http://dx.doi.org/10.1016/j.neures.2017.04.001. [PubMed: 28400206]

Sakai T, Mikami A, Suzuki J, Miyabe-Nishiwaki T, Matsui M, Tomonaga M, Hamada Y, Matsuzawa T, Okano H, Oishi K. Developmental trajectory of the corpus callosum from infancy to the juvenile stage: Comparative MRI between chimpanzees and humans. PLoS One. 2017b Jun. 12(6):e0179624. [PubMed: 28654656]

Sauleau P, et al. The pig model in brain imaging and neurosurgery. Animal. 2009; 3(8):1138–1151. [PubMed: 22444844]

Schiavone F, et al. Imaging age-related cognitive decline: a comparison of diffusion tensor and magnetization transfer MRI. J Magn Reson Imaging. 2009; 29(1):23–30. [PubMed: 19097099]

Schmithorst VJ, et al. Correlation of white matter diffusivity and anisotropy with age during childhood and adolescence: a cross-sectional diffusion-tensor MR imaging study. Radiology. 2002; 222(1): 212–218. [PubMed: 11756728]

Schomberg DT, et al. Miniature swine for preclinical modeling of complexities of human disease for translational scientific discovery and accelerated development of therapies and medical devices. Toxicol Pathol. 2016; 44(3):299–314. [PubMed: 26839324]

Schwerin SC, et al. Establishing the ferret as a gyrencephalic animal model of traumatic brain injury: optimization of controlled cortical impact procedures. J Neurosci Methods. 2017; 285:82–96. [PubMed: 28499842]

Smart IH, McSherry GM. Gyrus formation in the cerebral cortex in the ferret. I. Description of the external changes. J Anat. 1986; 146:141–152. [PubMed: 3693054]

Smith SM, et al. Advances in functional and structural MR image analysis and implementation as FSL. Neuroimage. 2004; 23(Suppl 1):S208–219. [PubMed: 15501092]

Smith SM, et al. Tract-based spatial statistics: voxelwise analysis of multi-subject diffusion data. Neuroimage. 2006; 31(4):1487–1505. [PubMed: 16624579]

Song SK, et al. Diffusion tensor imaging detects and differentiates axon and myelin degeneration in mouse optic nerve after retinal ischemia. Neuroimage. 2003; 20(3):1714–1722. [PubMed: 14642481]

Song SK, et al. Demyelination increases radial diffusivity in corpus callosum of mouse brain. Neuroimage. 2005; 26(1):132–140. [PubMed: 15862213]

Stricker-Krongrad A, Shoemake CR, Bouchard GF. The miniature swine as a model in experimental and translational medicine. Toxicol Pathol. 2016; 44(4):612–623. [PubMed: 27073085]

Sukstanskii AL, Ackerman JJ, Yablonskiy DA. Effects of barrier-induced nuclear spin magnetization inhomogeneities on diffusion-attenuated MR signal. Magn Reson Med. 2003; 50(4):735–742. [PubMed: 14523959]

Sukstanskii AL, Yablonskiy DA, Ackerman JJ. Effects of permeable boundaries on the diffusion-attenuated MR signal: insights from a one-dimensional model. J Magn Reson. 2004; 170(1):56–66. [PubMed: 15324758]

Susuki K. Node of Ranvier disruption as a cause of neurological diseases. ASN Neuro. 2013; 5(3): 209–219. [PubMed: 23834220]

Swindle MM, et al. Swine as models in biomedical research and toxicology testing. Vet Pathol. 2012; 49(2):344–356. [PubMed: 21441112]

Takahashi M, et al. Magnetic resonance microimaging of intraaxonal water diffusion in live excised lamprey spinal cord. Proc Natl Acad Sci U S A. 2002; 99(25):16192–16196. [PubMed: 12451179]

Tao JD, et al. Histopathologic correlation with diffusion tensor imaging after chronic hypoxia in the immature ferret. Pediatr Res. 2012; 71(2):192–198. [PubMed: 22258131]

Torres LB, et al. The use of new world primates for biomedical research: an overview of the last four decades. Am J Primatol. 2010; 72(12):1055–1061. [PubMed: 20626038]

Vaishnavi SN, et al. Regional aerobic glycolysis in the human brain. Proc Natl Acad Sci U S A. 2010; 107(41):17757–17762. [PubMed: 20837536]

VandeBerg JL, Williams-Blangero S. Advantages and limitations of nonhuman primates as animal models in genetic research on complex diseases. J Med Primatol. 1997; 26(3):113–119. [PubMed: 9379477]

Veraart J, et al. Denoising of diffusion MRI using random matrix theory. Neuroimage. 2016a; 142:394–406. [PubMed: 27523449]

Veraart J, et al. Gibbs ringing in diffusion MRI. Magn Reson Med. 2016b; 76(1):301–314. [PubMed: 26257388]

Veraart J, Fieremans E, Novikov DS. Diffusion MRI noise mapping using random matrix theory. Magn Reson Med. 2016c; 76(5):1582–1593. [PubMed: 26599599]

Weinberger DR, Lipska BK. Cortical maldevelopment, anti-psychotic drugs, and schizophrenia: a search for common ground. Schizophr Res. 1995; 16(2):87–110. [PubMed: 7577773]

Welker, W. Why does cerebral cortex fissure and fold? A review of determinants of gyri and sulci. In: Jones, EG., Peters, A., editors. Cerebral Cortex. Vol. 8B: Comparative Structure and Evolution of Cerebral Cortex, Part II. Springer; New York: 1990. p. 3-136.

Wen Q, Chklovskii DB. Segregation of the brain into gray and white matter: a design minimizing conduction delays. PLoS Comput Biol. 2005; 1(7):e78. [PubMed: 16389299]

Wernersson R, et al. Pigs in sequence space: a 0: *66X coverage pig genome survey based on shotgun sequencing.* BMC Genom. 2005; 6:70.

Wright SN, et al. Perfusion shift from white to gray matter may account for processing speed deficits in schizophrenia. Hum Brain Mapp. 2015; 36(10):3793–3804. [PubMed: 26108347]

Wu YC, et al. Age- and gender-related changes in the normal human brain using hybrid diffusion imaging (HYDI). Neuroimage. 2011; 54(3):1840–1853. [PubMed: 20932911]

Wu D, et al. In vivo high-resolution diffusion tensor imaging of the mouse brain. Neuroimage. 2013; 83:18–26. [PubMed: 23769916]

Xu G, et al. Axons pull on the brain, but tension does not drive cortical folding. J Biomech Eng. 2010; 132(7):071013. [PubMed: 20590291]

Yakovlev, PI., Lecours, A-R. The Myelogenetic Cycles of Regional Maturation of the Brain, in Regional Development of the Brain in Early Life. Minkowski, A., editor. Blackwell Scientific Publications; Oxford: 1967. p. 3-65.

Zhang J, et al. Characterization of mouse brain and its development using diffusion tensor imaging and computational techniques. Conf Proc IEEE Eng Med Biol Soc. 2006; 1:2252–2255. [PubMed: 17946946]

Appendix A. Supplementary data

Supplementary data associated with this article can be found, in the online version, at https://doi.org/10.1016/j.jneumeth.2017.12.017.

HIGHLIGHTS

- An advanced diffusion weigted imaging protocol was used to map adolescent brain development in miniture pig.

- Longitudinal effects of aging were readily observed for whole-brain and regional diffusion metrics.

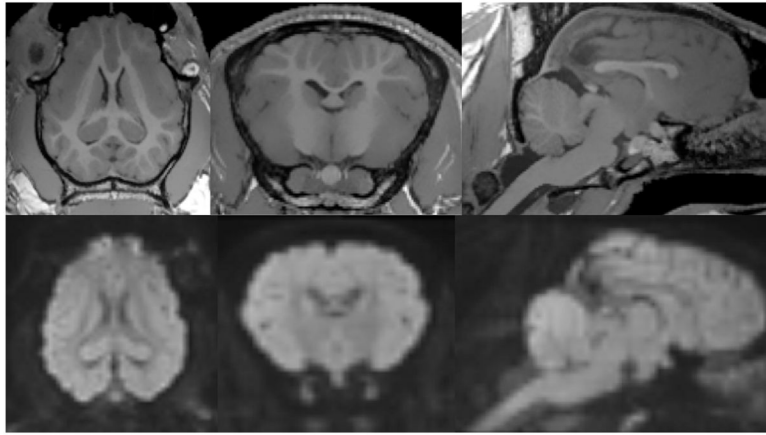- Regional diffusion metrics showed the expected heterochronic developmental patterns.

Fig. 1.
T1-weighted and DWI-weighted (average across all b-value) images collected in a live pig. T1-weighted image demonstrates fully gyrified cortex with excellent gray matter/white matter contrast. DWI-weighted image demonstrates excellent resolution and lack of shape distortion artifacts.
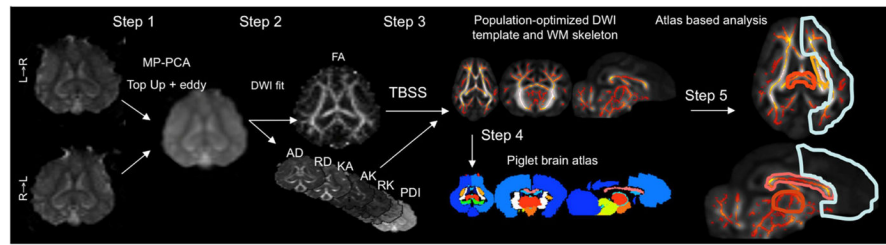
Fig. 2.
Analysis of DWI data. DWI data collected with reversal of phase-encoding gradients was denoised using MP-PCA filtering and corrected for shape distortions using TopUp and eddy current corrections (Step 1). In step 2, DWI model parameters were estimated including Fractional Anisotropy (FA) and Axial and Radial Diffusivity (AD and RD), Kurtosis Anisotropy (KA), Axial and Radial Kurtosis (AK and RK) and Permeability Diffusivity Index (PDI). Tract-based spatial statistics (TBSS) approach was used to warp individual FA images to a population-optimized FA atlas and project the center of the major WM tracts on the population-wide skeleton (Step 3). The other DWI parameters were projected on the skeleton based on FA projection maps for each subject (Step3). A piglet-based brain atlas was used to register the DWI brain template (Step 4). The overlap between regions of interests provided by the atlas and the skeleton of the cerebral white matter was used to calculate the regional average DWI parameters (Step 5).
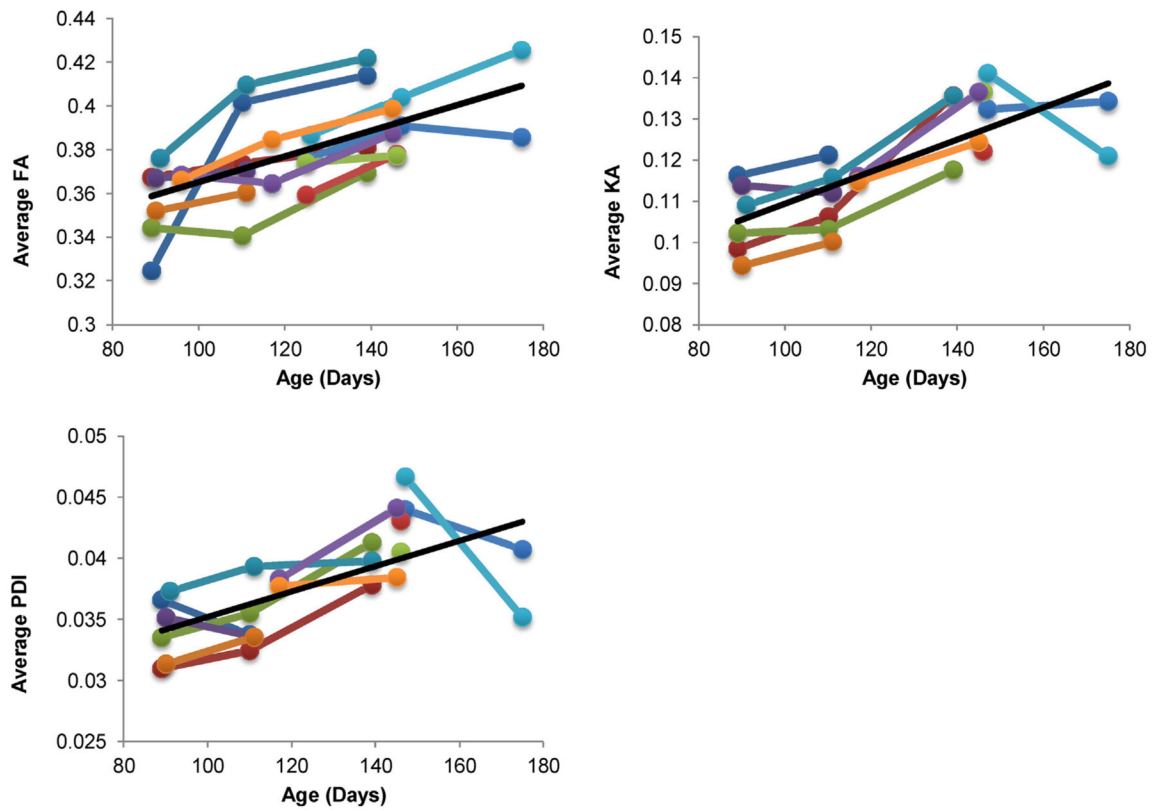
Fig. 3.
Average whole-brain Fractional Anisotropy (FA), Kurtosis Anisotropy (KA), and
Permeability-diffusivity index (PDI) showed significant longitudinal effects of age. The
fitted regresson line is shown in black. The average whole-brain diffusion trajectory for each
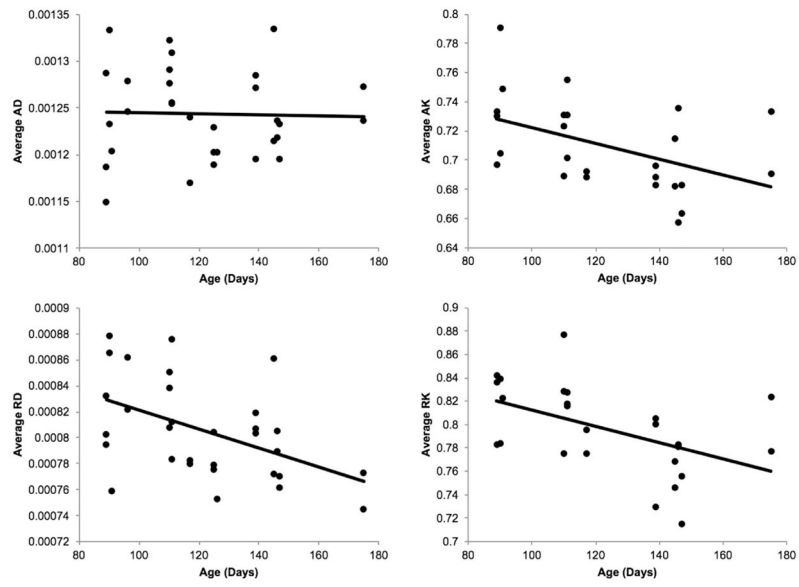individual pig is shown in color.

Fig. 4.
Average whole-brain AD, RD, AK, and RK diffusion measures versus age (days). AK and RK showed suggestive significance with age (p = 0.02). The fitted regression line is indicated in black.

Table 1

Fixed factor regression results (beta ± standard error (SE) and p-values).

Measurement	β_{Age} ± SE	p-value
DTI Model		
FA	**6.22E-04 ± 1.18E-04**	**1.46E-05**
AD	2.52E-07 ± 3.50E-07	0.54
RD	−4.13E-07 ± 2.29E-07	0.24
DKI Model		
KA	**3.89E-04 ± 6.91E-05**	**1.28E-05**
AK	**−5.21E-04 ± 2.19E-04**	**0.027**
RK	**−6.26E-04 ± 2.60E-04**	**0.025**
PDI Model		
PDI	**1.04E-04 ± 2.49E-05**	**3.71E-04**

Note: Bolded values indicate significance.

Author Manuscript

Author Manuscript

Author Manuscript

Author Manuscript

Table 2

Regional WM regression results for the fixed factors (beta ± standard error (SE) and p-values).

Region	FA β_{Age} ± SE (p-value)	AD β_{Age} ± SE (p-value)	RD β_{Age} ± SE (p-value)	KA β_{Age} ± SE (p-value)	AK β_{Age} ± SE (p-value)	RK β_{Age} ± SE (p-value)	PDI β_{Age} ± SE (p-value)
Corpus Callosum	**7.59E-04 ± 1.46E-04 (2.28E-05)**	-2.97E-07 ± 9.78E-07 (0.79)	-1.22E-06 ± 7.32E-07 (0.24)	**4.36E-04 ± 9.61E-05 (2.10E-04)**	-4.24E-04 ± 2.90E-04 (0.16)	*-5.37E-04 ± 2.36E-04 (0.04)*	**1.48E-04 ± 2.13E-05 (5.35E-07)**
Superficial WM	**5.71E-04 ± 1.12E-04 (2.33E-05)**	3.77E-07 ± 2.91E-07 (0.33)	-1.31E-07 ± 1.78E-07 (0.58)	**2.68E-04 ± 7.17E-05 (1.13E-03)**	*-5.33E-04 ± 2.19E-04 (0.02)*	-4.17E-04 ± 2.48E-04 (0.11)	**8.87E-05 ± 2.51E-05 (1.87E-03)**
Fornix/Parahippocampal WM	1.60E-04 ± 1.89E-04 (0.40)	-8.01E-07 ± 7.53E-07 (0.39)	-5.96E-07 ± 5.25E-07 (0.31)	1.57E-04 ± 1.52E-04 (0.31)	1.30E-04 ± 3.14E-04 (0.68)	3.70E-04 ± 3.17E-04 (0.26)	3.43E-05 ± 3.30E-05 (0.31)
Midbrain	**7.96E-04 ± 1.41E-04 (4.19E-06)**	2.50E-07 ± 6.31E-07 (0.73)	-7.42E-07 ± 5.00E-07 (0.20)	**4.83E-04 ± 1.36E-04 (1.73E-03)**	*-5.47E-04 ± 2.39E-04 (0.03)*	**-1.68E-03 ± 3.50E-04 (7.47E-05)**	**1.60E-04 ± 4.10E-05 (7.03E-04)**
Thalamic Radiation	**4.32E-04 ± 1.03E-04 (2.45E-04)**	1.40E-07 ± 3.50E-07 (0.72)	-3.16E-07 ± 2.86E-07 (0.38)	**8.32E-04 ± 1.32E-04 (1.96E-06)**	*-9.31E-04 ± 3.17E-04 (0.01)*	**-1.46E-03 ± 3.85E-04 (9.54E-04)**	**2.18E-04 ± 4.38E-05 (4.96E-05)**
Internal/External Capsules	**8.32E-04 ± 1.45E-04 (6.13E-06)**	8.27E-07 ± 3.66E-07 (0.14)	-4.74E-07 ± 2.23E-07 (0.19)	**6.28E-04 ± 1.90E-04 (3.20E-03)**	*-7.34E-04 ± 2.89E-04 (0.02)*	7.79E-05 ± 4.23E-04 (0.86)	5.57E-05 ± 2.83E-05 (0.06)

Note: Bolded values indicate significance and italicized values indicate suggestive (.007 < p ≤ .05) significance after correcting for multiple (N = 7 brain regions of interest) comparisons.